DOI: 10.13009/EUCASS2017-523

Development of a Probe for Particle Collection in High-Temperature, Supersonic Flow:

Application of Quasi-1D engineering model and 2D axisymmetric CFD

*F. Maggi*ⱡ, R. Bisin*, A. Ferreri*, S. Carlotti*, L. Galfetti*, C. Groll[§], T. Langener[§]*

** Politecnico di Milano, Dept. Aerospace Science and Technology*
Via La Masa 34, Milan, Italy

[§] ESA, Aerothermodynamics and Propulsion Analysis Section (TEC-MPA)
Keplerlaan 1, Noordwijk, The Netherlands

filippo.maggi@polimi.it· riccardo.bisin@mail.polimi.it · stefania.carlotti@polimi.it · luciano.galfetti@polimi.it
christopher.groll@esa.int · tobias.langener@esa.int

ⱡ:corresponding author

Abstract

The EMAP (Experimental Modelling of Alumina Particulate in Solid Booster) activity is a project funded under ESA's Basic Technology Research Program (TRP) for the characterization of the plume exhausted from a metalized solid rocket motor and measurement technique improvement. In this framework, the development of a probe for supersonic high-temperature flows was accomplished by the Space Propulsion Laboratory of Politecnico di Milano (SPLab-POLIMI). As a part of this activity, a joint effort was conducted between ESA and SPLab-POLIMI to fully assess the fluid dynamics of the supersonic internal flow governing the probe behavior. The simulation campaign was based on a twofold approach. A quasi 1-D solver based on steady-state compressible equation set in the form proposed by Shapiro was developed to obtain a smart engineering approach featured by low computational demands. On the same nominal geometry a hybrid 2D axial-symmetric mesh was generated and the turbulent flow field was solved using the DLR TAU CFD code. This paper aims at presenting the comparison between the results obtained from the aforementioned approaches.

Nomenclature

Symbols

A	Area
C_p	specific heat at constant pressure
C_v	specific heat at constant volume
c	speed of sound
D	hydraulic diameter
f	Fanning friction factor
k	specific heat ratio
L	length
L^*	mixing length
M	Mach number
M_m	molar mass
$\dot{m}$	mass flow rate
P	static pressure
P_t	total pressure
Q	heat
R	Universal gas constant
R_{gas}	Gas constant
Re	Reynolds number
s	entropy
x	distance along the probe axis
X_{vap}	fraction of evaporated mass
y	ratio V/V'_g
y	radial distance from the axis
y^+	dimensionless wall spacing
ρ	density

Acronyms

CFD	computational fluid dynamics
EMAP	Experimental Modelling of Alumina Particulate in Solid Booster
ODE	ordinary differential equation
TRP	Technology Research Program

Subscripts and superscripts

‘	forward component
cool	cooling flow
g	cooling gas
in	inlet
mix	ref. to mixing duct
quench	quenching fluid
tip	ref. to the tip

Copyright © 2017 by F. Maggi et al. Published by the EUCASS association with permission.

DOI: 10.13009/EUCASS2017-523

T	temperature	vap	evaporated flow
V	velocity	wall	ref. to a wall
W	work		

1. Introduction

In the frame of the EMAP project, an ESA-funded TRP program lead by DLR, the Space Propulsion Laboratory (SPLab) of Politecnico di Milano (POLIMI) was in charge of developing a collector to be placed close to the nozzle exit of a solid rocket motor. This intrusive probe aims at collecting the condensed combustion products present in the supersonic exhaust. The construction scheme and the conceptual work flow of the system are reported in Figure 1. The detailed description of the design and testing process is part of another paper presented in this same conference [1].

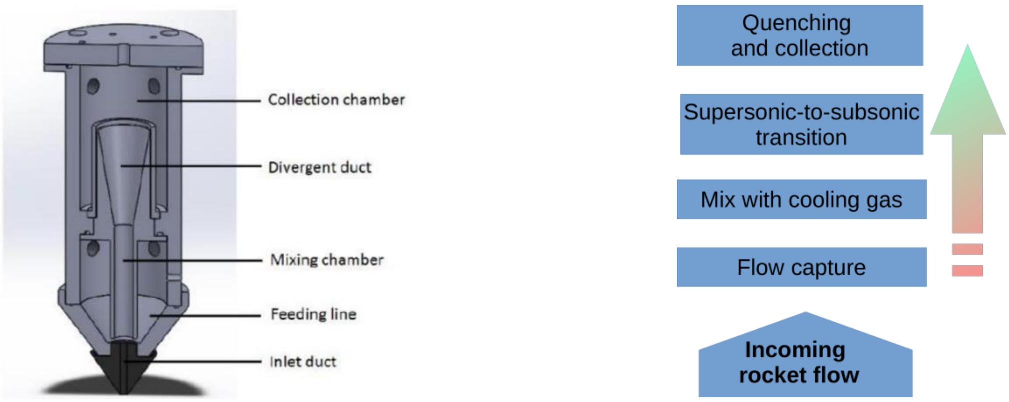

a) Construction scheme. b) Logical work flow.

Figure 1: The supersonic collection probe

The probe operates as internal supersonic diffusor. The flow coming from the external supersonic rocket nozzle is captured by the straight inlet duct, drilled in a graphite tip. After that, a radial injection enables the mixing between the ingested hot stream and nitrogen gas, used as a diluting coolant at ambient temperature. A channel follows, ensuring the time and space for complete mixing. Finally, the flow enters a conical divergent channel (divergent duct) where a shock wave is expected to occur. The location of the shock in this variable-area channel section is dictated by the adverse pressure that settles in the final collection chamber, where a set of calibrated exhaust nozzles allows to control the flow-rate to the ambient. The local stagnation pressure is defined by the steady-state mass balance of this chamber. Inside the collection volume, a liquid spray captures the incoming particles and makes them settle in an annular reservoir. According to the concept, the flow enters and moves inside the probe as supersonic, up to the internal divergent truncated cone (divergent duct).

A complex external-internal fluid dynamic design concept has been implemented to ensure that the flow is captured in the supersonic regime and, then, progressively cooled and decelerated before the supersonic-to-subsonic transition. The probe is acting as an internal-flow supersonic diffuser so it requires to start. During the initial transient a bow shock is expected to settle in front of the inlet. This condition is representative of a subsonic flow in the inlet duct. The reasons for this occurrence may be two-fold. On the one side, the bow shock can be generated by the external conical shape of the tip if no solution for an attached oblique shock is possible at the given cone angle and Mach number. Furthermore, this can also be influenced by blunt edges at the inlet, and hence require the probe tip to be designed with sharp edges. On the other side, the front shock may be generated by adverse pressure in the channel, if the fluid dynamic conditions impose an internal subsonic flow [2]. During regular operation the probe should feature an oblique shock wave attached at the inlet lip and at the tip channel, maintaining a supersonic core flow.

The fluid dynamic design has been conducted using a simplified quasi-1D solver named POLIRocket-V2 and based on steady-state, viscous, compressible flow equations in a form proposed by Shapiro [3]. This modeling tool was implemented to support the engineering choices and to produce a Monte Carlo analysis of the probe's off-design behavior. At the same time, ESA performed a CFD verification campaign using the DLR TAU solver. The comparison between the results in some peculiar operating cases gave the sensitivity of the reliability limits regarding the simplified Shapiro approach in such a complex scenario.

DOI: 10.13009/EUCASS2017-523

2. The POLIRocket-V2 code

The POLIRocket-V2 code is derived from a first implementation specialized in solid rocket motor internal ballistics [4]. The software is based on a set of quasi-1D, steady-state, compressible gas dynamic equations where continuity, momentum, and energy are conserved. The form of the equations used in this solver have been developed by Asher H. Shapiro, who presented a method to deal with complex fluid dynamic problems in which all variables vary primarily along one direction. Shapiro obtained a unique and comprehensive analytical tool capable of accounting for different phenomena such as area variation, wall friction, heat exchange, chemical reaction, change of phase, mixing of gases which are injected into the main stream, as well as changes in molecular weight and specific heat. The resulting equation set consists of 8 ODE relations, in logarithmic differential form, and 14 variables, six of them being independent.

State equation
$$\frac{dP}{P}=\frac{d\rho}{\rho}+\frac{dT}{T}-\frac{dM_m}{M_m} \tag{1}$$

Speed of sound
$$2\frac{dc}{c}=\frac{dk}{k}+\frac{dT}{T}-\frac{dM_m}{M_m} \tag{2}$$

Mach number
$$\frac{dM^2}{M^2}=\frac{dv^2}{v^2}+\frac{dM_m}{M_m}-\frac{dk}{k}-\frac{dT}{T} \tag{3}$$

Continuity
$$\frac{d\dot{m}}{\dot{m}}=\frac{d\rho}{\rho}+\frac{dA}{A}+\frac{dv}{v} \tag{4}$$

Energy eq.
$$\frac{dQ-dW+dH}{C_pT}=\frac{dT}{T}+\frac{k-1}{2}M^2\frac{dv^2}{v^2} \tag{5}$$

Momentum
$$\frac{dP}{P}+\frac{kM^2}{2}\frac{dv^2}{v^2}+\frac{kM^2}{2}\left(4f\frac{dx}{D}+\frac{dX}{\frac{1}{2}kPAM^2}\right)+kM^2(1-y)\frac{d\dot{m}}{\dot{m}}=0 \tag{6}$$

Impulse function
$$\frac{dF}{F}=\frac{dA}{A}+\frac{dP}{P}+\frac{kM^2}{1+kM^2}\frac{dM^2}{M^2}+\frac{kM^2}{1+kM^2}\frac{dk}{k} \tag{7}$$

2nd law of thermodynamics
$$\frac{ds}{C_p}=\frac{dT}{T}-\frac{k-1}{k}\frac{dP}{P} \tag{8}$$

The system can be rearranged to obtain a space-marching solution. Physical problems having a strong one-dimensional transport nature can take advantage of such a formulation. Rayleigh flow and Fanno flow models are restricted cases of the more general Shapiro equation set. Once the differential formulation is rearranged in terms of the so-called “influence coefficients”, the implementation of a solver becomes straightforward. The main drawbacks of this approach are a critical sensitivity to M = 1 causing numerical instability and an underlying continuity requirement for variables. However, specific workarounds can be implemented. For details, the reader is encouraged to consult the original book by Shapiro [3].

3. The TAU code

The numerical calculations presented here have been performed with the hybrid structured/unstructured DLR-Navier-Stokes CFD solver TAU [5]. Here, a second order finite-volume flow solver is applied to the RANS equations while the application of the AUSMDV flux splitting scheme, in tandem with MUSCL gradient reconstruction, enables second order spatial accuracy. Turbulence modelling is implemented by means of the Spalart-Allmaras one-equation eddy viscosity model. The gas in the calculations presented here is considered as non-reacting, ideal gas.

4. The test case

Now that the principle of the probe is established and the two analysis tools are introduced, this section describes the setup of the calculations whose results are compared in the following section.

DOI: 10.13009/EUCASS2017-523

4.1 Domain and boundary conditions of Shapiro Code

The computation domain is based on the probe operational scheme reported in Figure 2. The flow is assumed to exit from an upstream rocket nozzle with a parallel direction with respect to the axis of the probe. As the flow encounters the tip, an oblique shock is generated externally, attached to the inlet lip. If a supersonic condition is stabilized in the probe inlet channel, the flow enters the central perforation, mixes with nitrogen, and moves across the mixing chamber and the diffuser, where a shock is generated. The final part of the diffuser is subsonic. The collection chamber is modeled as a pressurized vessel with inlets (the flow ingested by the probe and the gas/liquid spray from the quenching mechanism) and outlets (a set of calibrated exit choked nozzles). The internal total pressure coincides with the one generated by the internal shock and results from local mass-balance equilibrium.

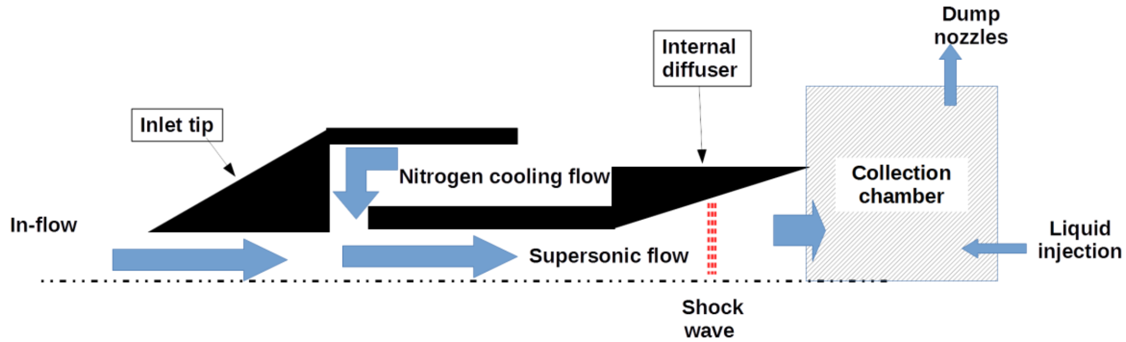

Figure 2: Internal scheme of probe design concept.

The POLIRocket-V2 code focuses on the internal channel flow. The computational domain is 1D and begins at the lip of the inlet duct. As the upstream flow is supersonic, the boundary conditions coincide with the themo-physical properties exiting from the upstream rocket nozzle, under the assumption of no present bow shocks. The nominal inlet data is reported in Table 1.

Table 1: Inlet properties for the design condition.

$M_{in} = 3.23$	$\rho_{in} = 0.0752\ kg/m^3$
$P_{in} = 53\ kPa$	$R_{gas} = 317\ J/(kg\ K)$
$M_m = 26.3\ g/mol$	$C_v = 1572\ J/(kg\ K)$
$T_{in} = 2227\ K$	$k = 1.20$
$C_p = 1888\ J/(kg\ K)$	$v = 2973\ m/s$

A description of the relevant components is given hereafter.

Inlet duct

The inlet duct is 3.5 cm long and has a diameter of 0.5 cm. The cross sectional area is constant. An improved version of the inlet is proposed in the second part of the paper, where the inlet rounding is introduced for better comparison with the TAU code. The flow is considered adiabatic. Friction effects are taken into account and locally evaluated by means of the typical curve fit equation, named after Blasius reported in Eq.(9) [6]. It is valid for $2.1 \times 10^3 < Re < 10^5$, where the channel is expected to have a nominal $Re = 17 \times 10^3$.

$$f = \frac{0.0791}{Re^{0.25}} \tag{9}$$

Mixing channel

The mixing duct is a constant-area channel with a diameter of 1.3 cm and a length of 8 cm. The main flow, arriving from the inlet, mixes with nitrogen cold gas injected into the main stream through a annular port which is assumed choked. The total properties of the nitrogen inlet are known so its mass flow rate can be defined. The mixing process in the channel is expected to slow and cool down the hot primary flow, resulting slightly supersonic flow at the inlet of the internal diffuser. The average properties of the fluid (specific heats, average molar mass) are recomputed locally. According to the Shapiro model, a mixing length L* is assumed. Such distance represents the length of the channel after which the flow is well stirred. The channel is adiabatic but non-isentropic due to friction. The total enthalpy of the main stream varies due to the addition of the inert coolant.

DOI: 10.13009/EUCASS2017-523

Divergent duct

At the exit section of the mixing chamber the flow is expected to be slightly supersonic. The divergent duct aims at cooling down the flow and slowing it down by means of a shock wave. This portion of the channel is 7.2 cm long with an exit diameter of 3.7 cm. The position of the discontinuity in the flow field depends on the backpressure generated in the collection chamber. The shock wave should be located at the beginning of the duct in order to limit the acceleration of the supersonic flow through the divergent. The position of the shock wave is computed through analytical process as proposed by Anderson in his textbook [7].

Collection quenching chamber

The flow resulting from the mixing of the ingested mass ($\dot{m}_{in-tip}$) and the nitrogen coolant ($\dot{m}_{in-cool}$) exits the divergent and dumps into the collection chamber. In this same volume, a liquid spray is introduced to capture the incoming particles inside a liquid suspension. The volume discharges into the external environment through 3 or 4 calibrated nozzles, maintaining a stable pressure during probe operation. This chamber is assumed to be under stagnation conditions so the total pressure in this volume corresponds to the one found downstream of the shock. According to the design specifications, the calibrated discharge nozzles are choked. The total pressure P_t is obtained from an internal mass balance of the collection chamber. The ideal discharge mass flow rate through the calibrated nozzles of known throat area A^* is proportional to the value of the total pressure, as represented in Eq.(10). In turn, the position of the shock (in terms of area ratio) rules the ratio of the total pressure across the discontinuity, as it depends on the upstream Mach number. The total temperature T_t as well as the specific heat ratio are assumed unchanged across the shock, despite static temperature variations. That is, the global equilibrium of the quenching chamber control volume is reached only by one specific value of the total pressure, which at the same time rules the mass flow rate discharged in the environment as well as the location of the shock. The real discharge mass flow rate should be weighted by a correction factor. For simplicity, it is initially assumed to be equal to unity.

$$\dot{m}_{id-dump} = A^* P_t \sqrt{\frac{\left\{k \left(\frac{2}{k+1}\right)^{(k+1)/(k-1)}\right\}}{R_{gas}\, T_t}} \tag{10}$$

When the injection of the quenching liquid is considered, the code assumes that part of it evaporates. The fraction X_{vap} is defined by the relation $\dot{m}_{quench-vap} = X_{vap}\, \dot{m}_{quench}$. The rest of the liquid $\dot{m}_{quench-liq} = \dot{m}_{quench} - X_{vap}\, \dot{m}_{quench}$ is assumed to accumulate in the collection chamber and is neglected in the mass-balance equation. The steady-state mass balance equation of the quenching chamber is reported in Eq. (11). Also, the enthalpy balance of the flow is modified to account for the mass addition of the quenching liquid and evaporation enthalpy contribution. During the design analysis the evaporated mass fraction is fixed to $X_{vap} = 0.5$.

$$\dot{m}_{id-dump} = \dot{m}_{in-cool} + \dot{m}_{in-tip} + \dot{m}_{quench-vap} \tag{11}$$

Algorithm of solution

The solution is based on trapezoidal rule second-order accuracy method, integrating an initial-value problem [8]. The code can be used in both design and off-design analysis. In the former case, the pressure in the collection chamber is set as design specification, deriving the rest of the probe properties (e.g. the exit area of the dump nozzles). In the latter case, geometric and inlet properties are fixed and the solver derives the new equilibrium pressure in the collection chamber. In both cases the local static properties are derived. A piece-wise solution strategy is adopted, requiring the variables to be continuous. The code is run from the tip to the shock and from the shock to the collection chamber. A constant discretization step is adopted, after proper sensitivity analysis. The code was numerically verified against different literature cases such as supersonic flow in presence of friction (Fanno flow model), heat addition (Rayleigh flow model), area variation (isentropic expansion), and global mass and enthalpy balance. The code maintains a good level of accuracy until the sonic condition is approached, when a singular point for the Shapiro formulation is present. A workaround for this condition was not implemented since a sonic point is not expected in the domain.

DOI: 10.13009/EUCASS2017-523

4.2 Numerical Setup Using the TAU Code

The computational domain used in the TAU calculations is derived from the cross section of the probe. Figure 3 shows the axisymmetric grid, which is generated for the probe geometry using the CENTAUR 11.5 hybrid grid generation package and subsequently refined by TAU's gradient-based mesh adaptation module. The grid consists of approximately 220000 nodes and employs prismatic layers in order to resolve boundary layers on viscous walls. These structured layers are adapted over the course of several computations, in order to ensure a dimensionless wall spacing of $y^+ = 1$. It is shown in Figure 5 that the adaptation process is successful in generating a mesh adhering to this goal. An adaptation process is also applied to the unstructured grid regions in order to increase the grid resolution at locations with substantial temperature, pressure and Mach number gradients using a mixed criterion. Figure 4 gives a detailed view of the grid within the inlet channel where the refined mesh reflects the complex flow at this location. The wall temperatures are fixed at $T_{wall} = 298K$. This 2D mesh is extruded to a 1 degree wide wedge bound by Euler walls, as no swirl is considered in this computation.

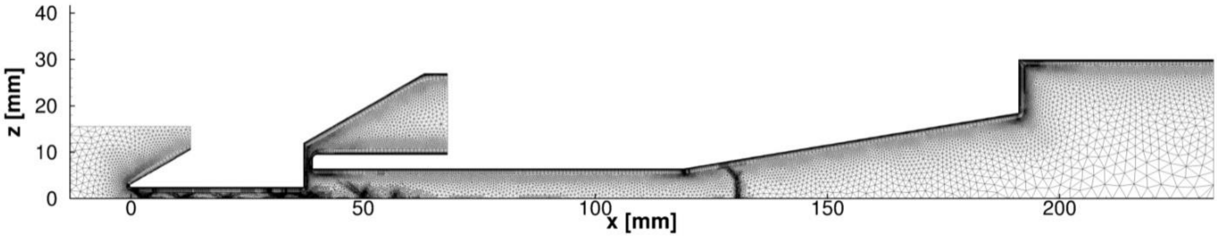

Figure 3 Mesh generated for TAU computations with 2 bar backpressure.

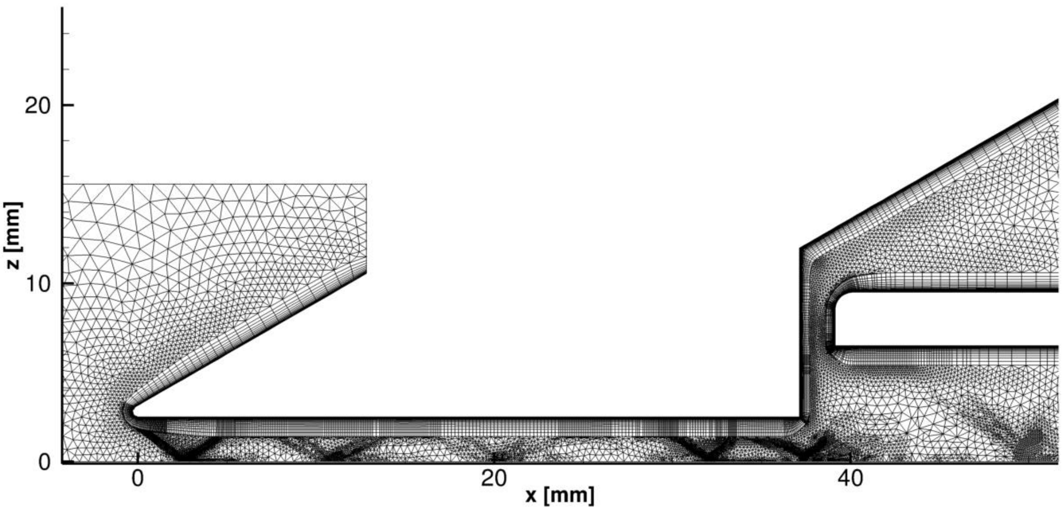

Figure 4 Detailed view of the adapted Mesh within the probe inlet and mixing duct for calculations with 2 bar backpressure.

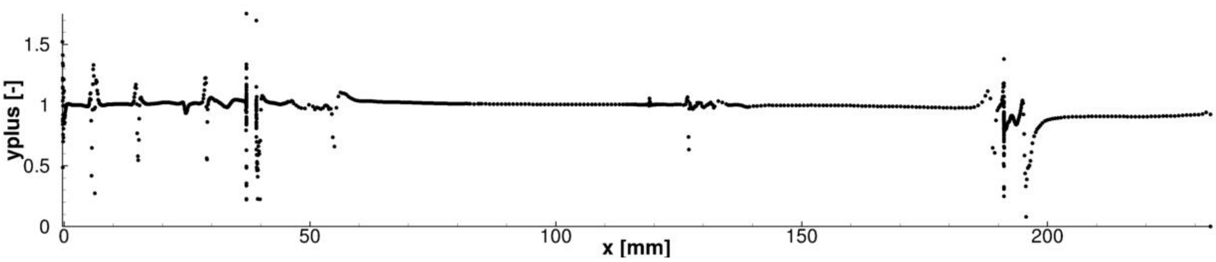

Figure 5 Plot of sampled y^+ values along the internal probe walls for the mesh shown in Figure 3 and Figure 4.

DOI: 10.13009/EUCASS2017-523

Upstream from the probe inlet, a far field boundary condition is employed to set up the flow encountered by the probe. The inlet conditions were estimated from computations using CEA and hence represent a simplified plume flow with M=3.36, p=53000 Pa and T=2226.7 K. For the reduction of the computational effort no further chemical reactions were considered in the CFD simulations and the free-stream gas adiabatic exponent was set to 1.16 and the gas constant 298 kJ/kg K. The flow then passes the inlet duct before encountering the radial coolant flow. The rotational geometry, used in the computation presented here, prohibits the inclusion of the discrete coolant injection points found in the real probe design. Therefore, only part of the coolant inlet plenum is modeled while the coolant input is realized by means of a reservoir-pressure inflow boundary condition on which the total pressure and total density of the coolant are fixed. The included inlet geometry then allows for the capturing of the effects caused by the redirection of the flow to the radial injection point. This represents a compromise between the low computational effort of quasi 2D calculations, which is desirable as a large number of coolant inlet and discharge pressure combinations are examined, and the inclusion of flow effects caused by the complex internal geometry of the probe. After passing the mixing channel and the divergent nozzle, the ingested gas and coolant mixture enters the collection chamber, which is simplified as a cylinder. Here again the discrete outlets of the probe, as shown in Figure 1, are neglected and the expulsion of gas is facilitated via a constant pressure outlet boundary condition. With this configuration it is possible to predefine the collector pressure, which in the probe hardware is set up via calibrated orifices. An overview of the described setup, as well as the selected inlet conditions, is given in Figure 6.

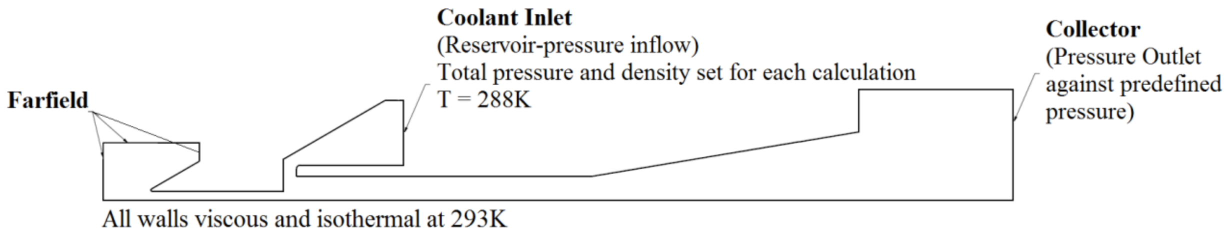

Figure 6 Overview of selected boundary conditions.
The far field is defined according to the values given in Table 1.

5. Results

5.1 POLIRocket-V2

The code was used to produce the design of the probe, fixing a quenching chamber pressure of 2 bar. The mass ratio between tip and the nitrogen flow rates is selected to 10.02, after some parametric analyses. The results obtained for the nominal operating condition (Table 1) are discussed in the following. Figure 7 reports the local Mach number, Figure 8 contains information about static temperature and pressure. The horizontal axis represents the coordinate inside the probe channel starting from the lip of the inlet tip. Three colors are identified in the figures, one per each part of the apparatus. The black curve represents the inlet duct. The inlet of the nitrogen cooling flow is placed at the end of this portion. The red curve corresponds to the mixing channel and the blue leg is representative of the internal divergent. The right-side end of the curve is the inlet condition for the quenching area.

In the first part a straight channel with friction is present. This is a Fanno flow and a decrement of the supersonic Mach number is expected. In this section the total temperature is preserved while the total pressure decreases, However, a general increment of the static properties is visible since a decrease of the local Mach number is recorded. In the second portion, the mixing is modeled as a progressive mass addition with corresponding increment of the main flow area. That is, in this portion the total properties vary locally, as the mixing process is distributed. Initially, the Mach number strongly decreases because of the momentum balance. Then, the mass injection and the temperature reduction (and thereby the reduction of the speed of sound) lead to a further slight increase. The static pressure can be interpreted in a similar manner while the static temperature progressively decreases because of the cooling effect of the injected flow (reduction of local speed of sound), and consequent reduction of the mixture total temperature. Finally, the divergent portion shows the typical behavior of an over-expanded nozzle modeled in a quasi-1D framework. A shock is located after an initial expansion and consequent acceleration. The Mach number sharply decreases, after an initial increment. The reported static properties increase. As design choice, the mass of

DOI: 10.13009/EUCASS2017-523

injected nitrogen maintains the temperature at the shock below the melting point of metallic aluminum (reportedly, below 933 K).

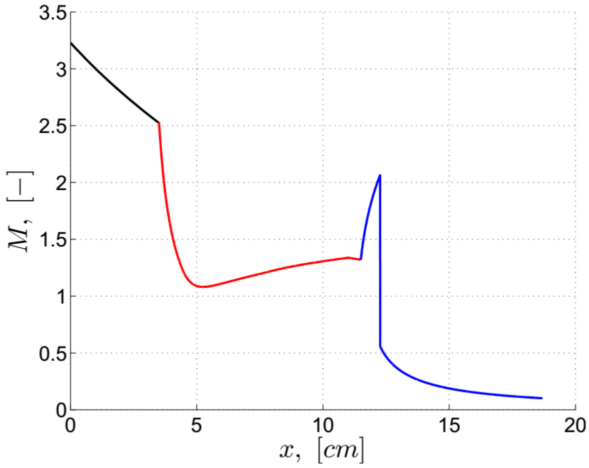

Figure 7: Local Mach number in the probe (POLIRocket-V2 code).

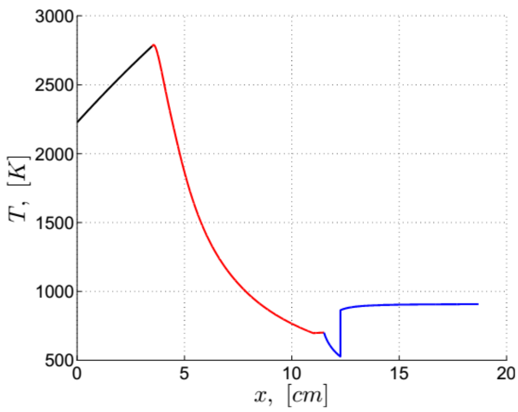

a) Static temperature

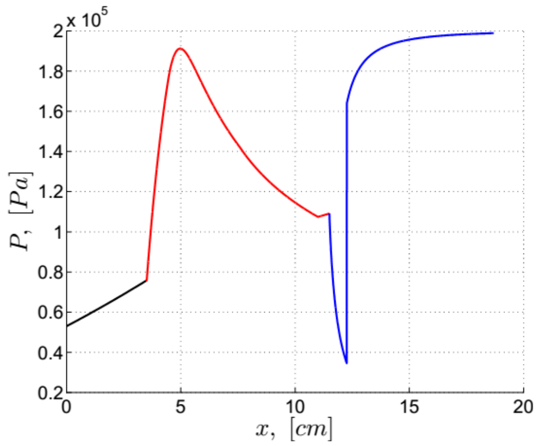

b) Static pressure

Figure 8: Local static thermodynamic properties in the probe (POLIRocket-V2 code).

Two examples of parametric analysis on the mixing process are reported in Figure 9.

In the case (a), the mass ratio between the nitrogen coolant flow and the inlet tip is varied. The progressive increment of the coolant injection decreases the minimum Mach number obtained in the mixing duct. Locally the value of M = 1 is approached but not reached. At the same time, the location of the shock is shifted downstream.

In case (b) the variation of the mixing length L* is explored. As already discussed, this number is a parameter which should be selected with some criteria. The design cases have been run using a mixing length of 7.5 cm, equivalent to $L^* = 0.938\ L_{mix}$. The results show that only the flow in the mixing duct is sensitive to this selection. The longer the L*, the smoother the variation of the thermodynamic and fluid properties. The end of the mixing process coincides with a local maximum of the Mach number. The minimum value of the Mach in the mixing channel and the location of the shock are quite insensitive to this parameter.

DOI: 10.13009/EUCASS2017-523

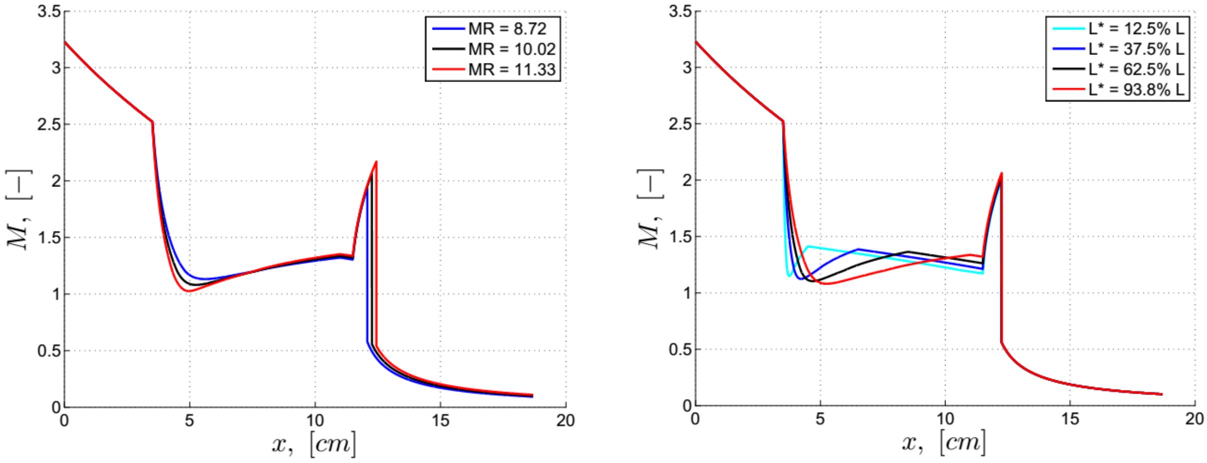

a) Mass ratio (L* = 7.5 cm). b) Mixing length (MR = 10.02).

Figure 9: Parametric studies on mixing process; the plots are representing the Mach number.

5.2 TAU code

Computations have been performed for a wide range of coolant inlet and collector pressure combinations, while the far field conditions remain constant throughout the results presented here. Several selected cases are discussed in the following. The goal is the identification of an operational point, which allows for the capture of Alumina particles from the hot exhaust flow without altering their size distribution. As the incoming particles are assumed to still be in their liquid phase it is necessary to limit their exposure to shocks, which might prompt them to break up, causing the size distribution of the ingested particles to vary from the one present in the free stream. Therefore the probe's internal pressure needs to be set to a value that allows the flow into the probe to start, avoiding the generation of a bow shock. Figure 10 shows a detailed view of the results obtained for a computation where the collector pressure outlet boundary condition is set to 7 bar while the total pressure at the coolant inlet boundary condition is also set to 7 bar in order to avoid flow out of the coolant inlet. It can be seen that hot gases do not enter the probe and that a bow shock is formed in front of the inlet because of cold gas escaping the probe through the inlet.

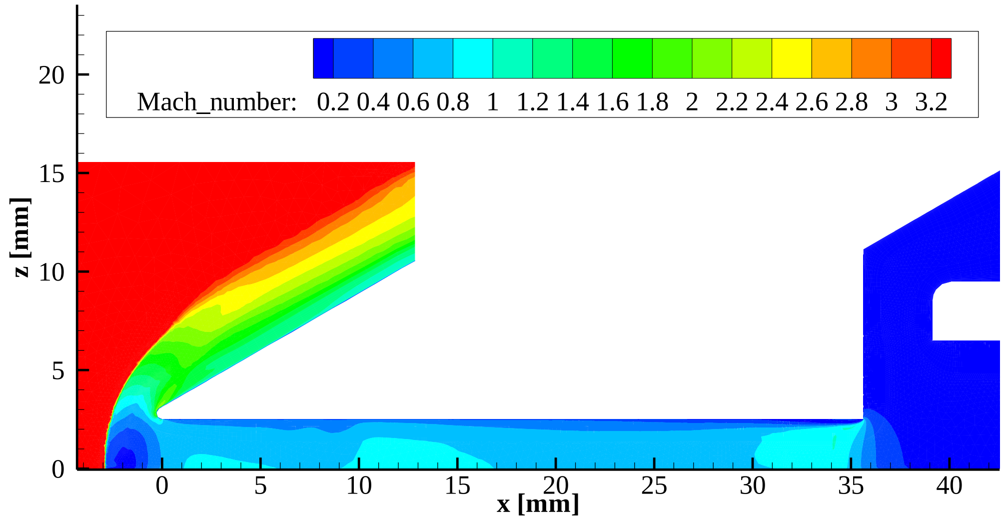

Figure 10 Detailed view of the probe inlet; a backpressure in excess of 7 bar prohibits the ingestion of hot gas and creates a bow shock in front of the probe inlet which may cause incoming liquid Alumina particles to break up.

Reducing the pressure prescribed at the outlet boundary condition to 6 bar results in the establishment of the flow field indicated in Figure 11. The inclination of the shock corresponds to the nominal behavior of a cone exposed to a supersonic flow [9]. As in several aeronautical internal-diffusion supersonic intakes, an oblique shock train is generated inside the inlet duct [10]. However, the flow is still supersonic and progressively slows down through a set of weak shocks. Towards the end of the duct a boundary layer separation can be identified on the flow region close to the walls but such event does not propagate upwards and does not choke the inlet channel. While the probe now ingests hot gases from the external flow, the transition to subsonic speeds takes place before the flow has the opportunity to mix with the radially injected coolant. It is therefore plausible to assume that the ingested particles are still in a liquid state when they enter a region with substantially lower gas velocity, making them susceptible to breakup.

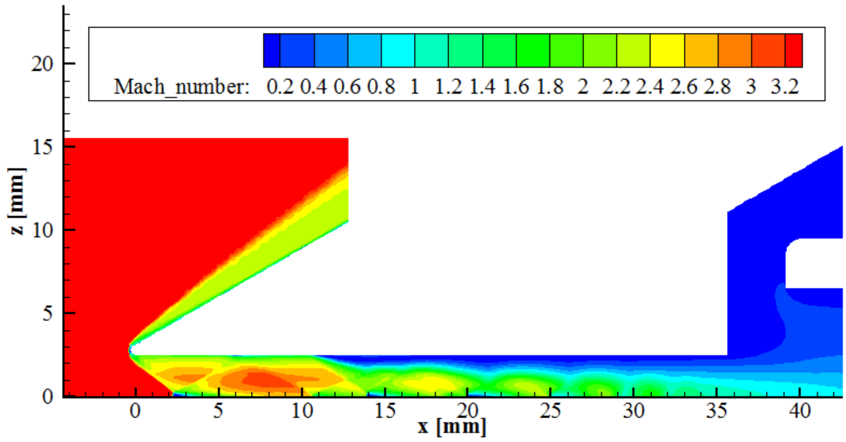

Figure 11 Flow field within the probe inlet for a backpressure of 6 bar.

Further reducing the backpressure to 4 bar while setting the coolant inlet condition to $p_{tot,coolant} = 4\ bar, \rho_{tot,coolant} = 4{,}66\ \frac{kg}{m^3}$ mitigates this issue. Figure 12 gives a detailed view of the shock train present in the inlet channel while Figure 13 gives an overview of the results for the entire domain. While the flow topology up to 10 mm downstream of the inlet remains identical to the 6 bar backpressure case, the flow remains sonic up to 70 mm downstream of the inlet. The transition to subsonic conditions is promoted by the addition of the coolant, which reduces the static temperature of the mixture flowing through the mixing chamber. Figure 14 gives an indication of the temperature of the ingested gas as it mixes with the radially injected coolant. The temperature in the core flow falls below the melting point of Alumina at approximately 70 mm downstream of the probe inlet. This gives the particles time to cool before they enter the collection chamber and interact with the fluid droplets that are being injected there.

Also note that the width of the coolant inlet is reduced in the 4 bar backpressure case in order to arrive at the intended coolant mass flow rates.

The backpressure is now further reduced to 2 bar, while leaving the coolant inlet condition unchanged, in an attempt to give the particles more time to cool down before they encounter a region of subsonic flow. The detailed view of the flow field in the inlet duct is shown in Figure 15. It can be seen that it is quite similar to that encountered in the 4 bar backpressure case. This is due to the radial injection of coolant just behind the inlet. The coolant impinges on itself, creating a zone of increased pressure, which limits the influence of downstream pressure variations on the inlet duct flow field. It can also be seen that the velocity within the radial cooling gas inlet increases due to the decreased pressure in the mixing duct. The overview plot of the Mach number in Figure 16 also shows that the bulk of the fluid passing the mixing duct stays supersonic and even accelerates when it reaches the divergent section of the duct. This is generally not desirable as the particles within the stream are to be stopped within the probe but the acceleration of the gas is accepted here as this pressure combination allows the particles to cool and solidify in a high velocity flow before entering the subsonic part of the probe. Figure 17 gives an insight into the temperature distribution within the flow. It can be seen that the length of the mixing channel is sufficient for the hot gas to mix with the injected cold gas before entering the collector.

DOI: 10.13009/EUCASS2017-523

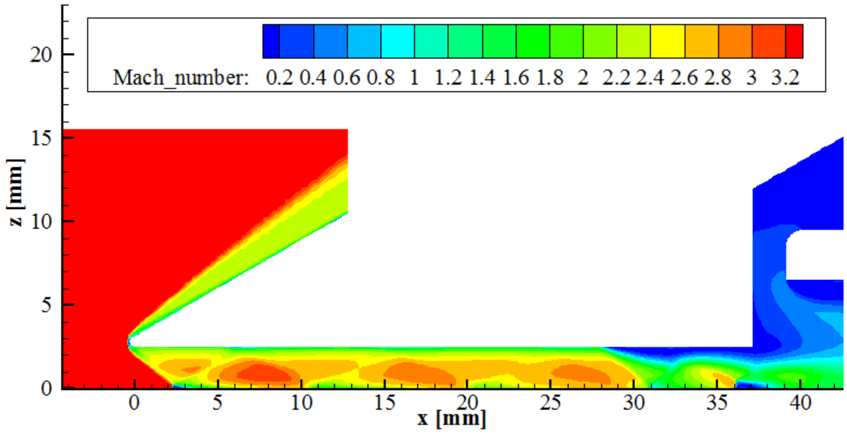

Figure 12 Flow field within the probe inlet for a backpressure of 4 bar.

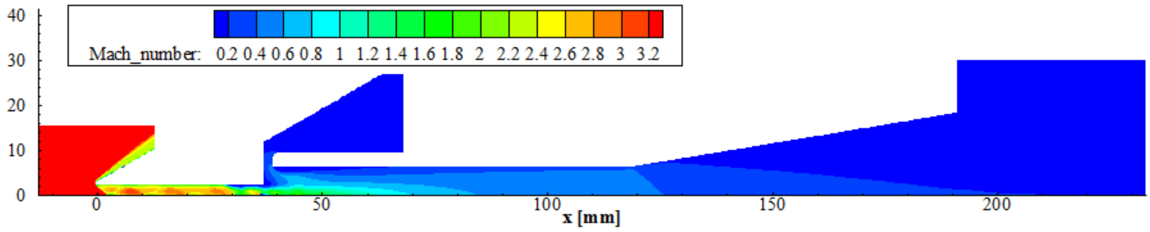

Figure 13 Overview of flow field at 4 bar backpressure.

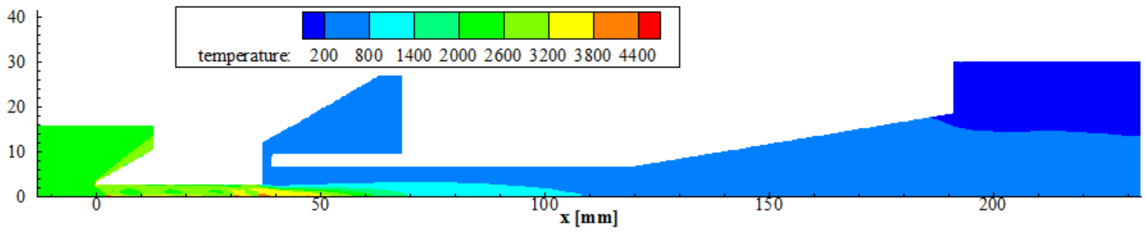

Figure 14 Plot of temperatures encountered within the probe for the 4 bar backpressure case.

DOI: 10.13009/EUCASS2017-523

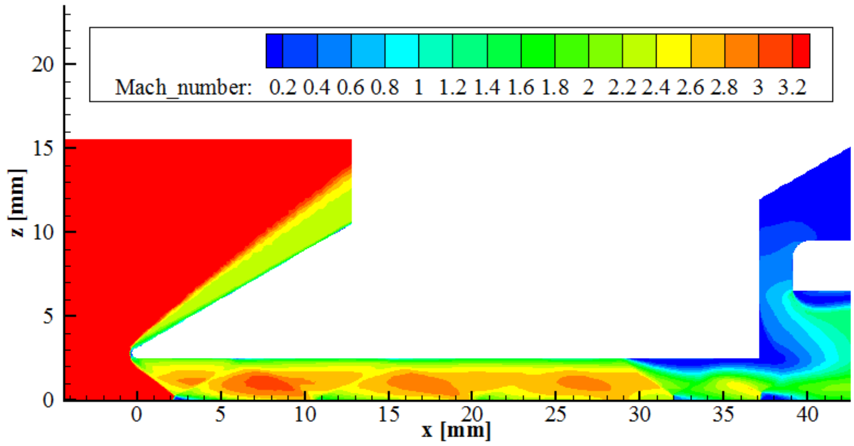

Figure 15 Detail of the flow field in the probe inlet for the case of 2 bar backpressure.

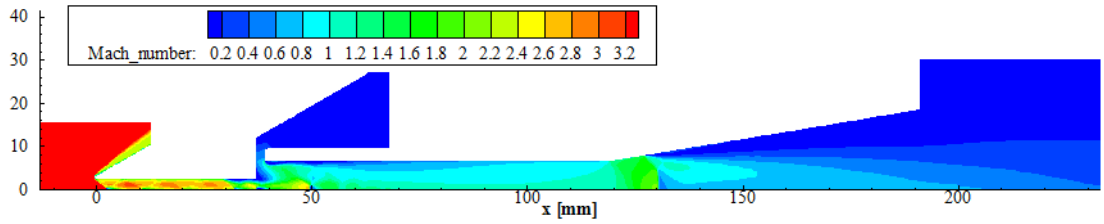

Figure 16 Overview of flow field at 2 bar backpressure.

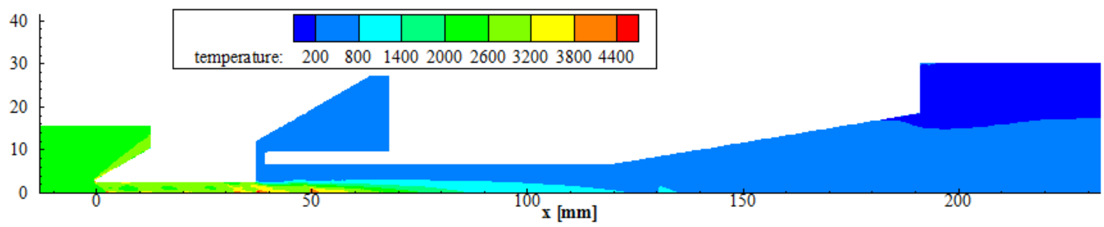

Figure 17 Plot of temperatures encountered within the probe for the 2 bar backpressure case.

DOI: 10.13009/EUCASS2017-523

6. Comparison and discussion

The simulations of the TAU code are now compared to the results generated by the POLIRocket-V2 code. The quasi1-D software was modified to include the inlet rounding effect as modelled in the 2D mesh. In both cases the same Mach number of $M = 3.36$, the same gas properties of $k = 1.16$ as well as $R_{gas} = 298\, J/(kg\, K)$ were adopted. The other thermodynamic properties were modified accordingly. This new condition enabled the same inlet mass flow rate through the tip. The POLIRocket-V2 code could not implement the nominal coolant-to-inlet mass ratio of 10.9 due to sonic point instability. The value was set to 10.4 for this code only. In addition to the cases discussed above simulations were performed with 1 bar and 3 bar backpressure and a coolant total pressure of 4 bar in order to gain two additional verification cases. Static pressure, static temperature, and Mach number data are extracted from TAU computations. Data sampling points are located on the rotational axis at one millimeter intervals throughout the internal probe flow path up to the end of the divergent duct. Due to the large variation of these variables over the radius of the flow passages, data averaged over the channel cross section is also extracted at identical axial positions. For the extraction of the static pressure the area averaging technique is used while temperature and Mach number averages are generated using a mass flow weighted averaging approach.

With respect to the Shapiro code, the CFD analysis ensures higher degree of details including turbulence modeling, oblique shock determination, and boundary layer development. On the other hand, the Shapiro code represents an appealing engineering approach due to its straightforwardness and low computational demands. Hence, these two approaches are complementary and a comparison between them is essential to assess the quality of the Shapiro code. The comparison of meaningful results is performed by showing both punctual data on the probe axis and the section-averaged values along the channel.

As shown in Figure 18 and Figure 19, the TAU code identifies a strong fluctuation along the inlet duct for Mach number, static temperature, and static pressure. This is caused by the oblique shock train in the inlet duct, visible also in Figure 12. The POLIRocket-V2 code cannot detect this event and presents a smooth behavior. When the TAU averaged properties are considered, the resulting Mach number in the inlet duct is lower than the one provided by the Shapiro approach. As a consequence, the temperatures and the pressures are higher. The trend can be justified by Mach number reduction introduced by the oblique shock pattern departing from the inlet, not visible by the quasi-1D approach.

Once the main flow reaches the mixing chamber, a sudden Mach number decrement is observed by the POLIRocket-V2 code because of the mixing with the cooling flow. The same process is visible in the CFD approach but data analysis is clearer when the curves with the averaged properties are considered. The injected coolant flow impinges on the main flow creating a subsonic region for the length of the mixing duct. The trend observed by the Shapiro approach is the same but also in this case an overestimation is obtained. The reader should remember that the POLIRocket-V2 code is introducing a lower coolant mass because the flow cannot reach sonic conditions for computational stability. For the divergent portion, both the codes agree on the definition of the shock wave location. The CFD analysis reveals the presence of oblique shocks in the divergent portion and the resulting pattern is not planar. Such details cannot be detected by the quasi-1D approach where this supersonic-to-subsonic transition is observed as a discontinuity.

Globally, the Shapiro approach features the same trend as the CFD results in terms of averaged quantities. However, some discrepancies are present. The flow presents a strong bi-dimensional property due to shock generation. The boundary layer is minimally influencing the condition under analysis. Another interesting point is represented by the effect of the coolant injection. According to the standard CFD approach, a subsonic region is present at the injection of the nitrogen, whereas the POLIRocket-V2 is forced to operate in the proximity of a sonic condition for numerical stability reasons, reducing the coolant mass flow rate. In any case, the trend matching is very good and the capability of capturing the shock wave location is valuable.

DOI: 10.13009/EUCASS2017-523

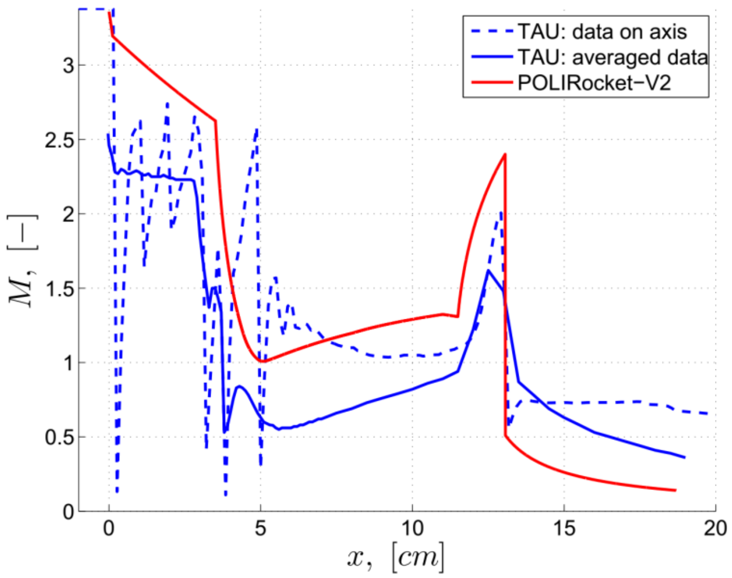

Figure 18: 2D axial-symmetric vs. quasi 1D comparison: Mach number.

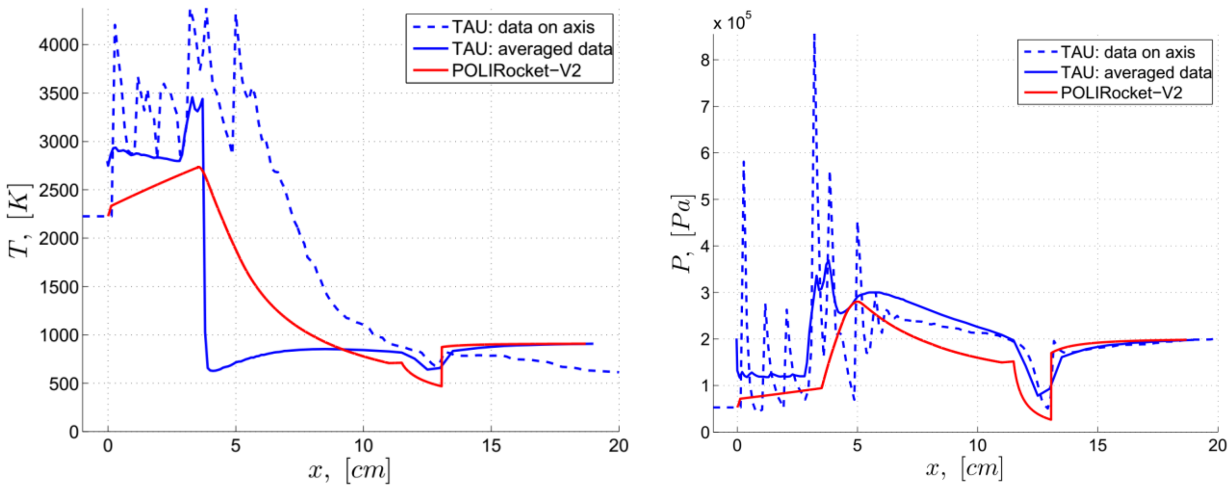

a) Static temperature

b) Static pressure

Figure 19: 2D axial-symmetric vs. quasi 1D comparison: thermodynamic properties.

6. Conclusions

The comparison between a quasi-1D code based on a mathematical approach proposed by Shapiro and axial-symmetric CFD calculations has been presented. A complex test case where an internal supersonic flow mixes with a cooling flow was considered. The comparison of Mach numbers, static pressure and static temperature was reported for the different flow regimes contained in the flow domain, including channel with friction, flow mixing, and overexpansion. A section-averaged comparison appears to be meaningful when using the axial-symmetric CFD data.

With respect to the CFD approach, the quasi-1D method is less detailed and is not capable of capturing fluid dynamic effects that develop transversally with respect to the flow direction. The variable trends are correctly captured. The absolute numbers of the variables are not the same but the trends are shifted one respect to the other. The variations of the flow properties are similar in both of the cases. Most of the problems arise in all the processes that are intrinsically multidimensional. Oblique weak shock waves are not identified, being intrinsically more-than-1D processes. As a consequence, pressure and temperature trends are smoother because shock trains are not captured. On the contrary, the location of normal shocks is properly captured. In the quasi-1D approach the mixing between two fluids seems to have a different duration between the two approaches. The reader should be aware that the flow mixing in the Shapiro approach requires a proper tuning for the length of the process and there is not a closed solution. In the presented case, it is clear that the stirring of the flow properties occurs faster than expected and a

DOI: 10.13009/EUCASS2017-523

proper iterative work is requested on the POLIRocket-V2 solver. As a general problem of this specific formulation of the problem, the sonic condition is a singular point without workaround implementations. Finally, the execution time of the proposed quasi-1D approach is orders of magnitude lower than a CFD solution. A direct comparison between the codes was not conducted, as they were run on heterogeneous computation systems. For this reason, the POLIRocket-V2 code was then used for Monte Carlo evaluations about the operational envelope of the probe.

In general, the approach proposed by Shapiro has a very low computational demand and demonstrates to be directly applicable in simple geometry cases. When more-than-1D processes develop within the flow, the code shows some limitations. Variable trends and variations are properly obtained even though the tuning of some processes is requested, under different flow regimes. As a general problem of this specific formulation of the problem, the sonic condition is a singular point and a workaround implementation is underway. In addition an activity for the tuning of different flow regimes and conditions with complete CFD solutions is progressing: miscible flow mixing, boundary layer growth, supersonic vs. subsonic cases represent some of the test cases that will be investigated in the near future.

Based on the application of the Shapiro code presented in this paper the design of the particle collection probe was finalized and the CFD simulations were used to contribute to define the final mode of operation for the use in a solid rocket motor exhaust plume.

References

1 S. Carlotti et al. Development of a Probe for Particle Collection in High-Temperature, Supersonic Flow: Conceptual and Detailed Design. *7th EUCASS*, Milan, 3-6 July, 2017.

2 S. Farokhi. *Aircraft Propulsion*, 2nd Edition. Wiley, 2014.

3 A.H. Shapiro. *Dynamics and Thermodynamics of Compressible Fluid Flow*, Vol. 1. John Wiley & Sons Inc., 1953.

4 D. Vigano, A. Annovazzi, and F. Maggi. Monte Carlo Uncertainty Quantification Using Quasi-1D SRM Ballistic Model. *International Journal of Aerospace Engineering*, Volume 2016 Article ID 3765796, 2016.

5 Anon. Homepage of DLR TAU code, http://tau.dlr.de/code-description/, last visit 13/06/2017.

6 R.B. Bird, W.E. Stewart, and E.N. Lightfoot. *Transport Phenomena*, 2nd Edition. Wiley, 2007.

7 J. D. Anderson. *Computational fluid dynamics: Basics with applications*. McGraw Hill, 1995.

8 W.H. Press et al. *Numerical Recipes: The Art of Scientific Computing*, 3rd Edition. Cambridge University Press, New York, USA, 2007.

9 J.D. Anderson. *Modern compressible flow: with historical perspective,* Second Edition. McGraw Hill, 1990.

10 K. Matsuo. Shock Train and Pseudo-Shock Phenomena in Supersonic Internal Flows. *Journal of Thermal Science*, 12(3):204-208,2003.